Hyperfine-mediated spin relaxation in donor-atom qubits in silicon

Yu-Ling Hsueh,[1,2] Ludwik Kranz,[1,2,3] Daniel Keith,[1,2,3] Serajum Monir,[1,2] Yousun Chung,[1,2,3] Samuel K. Gorman,[1,2,3] Rajib Rahman,[1,2] and Michelle Y. Simmons[2,3,*]

[1]*School of Physics, University of New South Wales, Sydney, NSW 2052, Australia*

[2]*Silicon Quantum Computing Pty Ltd., Level 2, Newton Building, UNSW Sydney, Kensington, NSW 2052, Australia*

[3]*Centre for Quantum Computation and Communication Technology, School of Physics, University of New South Wales, Sydney, NSW 2052, Australia*

(Received 12 February 2022; revised 25 January 2023; accepted 24 March 2023; published 20 April 2023)

Donor electron spin qubits hosted within nanoscale devices have demonstrated seconds-long relaxation times at magnetic fields suitable for the operation of spin qubits in silicon of $B = 1.5$ T. The relaxation rates of these qubits have been shown at milliKelvin temperatures to be mediated by spin-orbit coupling with a B^5 dependency on magnetic field for $B > 3$ T with a transition to a B^3 dependency at magnetic fields below ($B \leqslant 3$ T). This deviation has been observed in many spin qubit systems but is particularly notable in multidonor quantum dot qubits. The reason for this has remained a mystery. In this paper we show that for these multidonor low noise, crystalline qubits this deviation at low magnetic fields can be explained by a hyperfine mediated relaxation mechanism of the electron spin through a quantitative model of the relaxation rates. This model identifies the importance of donor nuclear spin flips which are more apparent in multidonor systems in which the larger numbers of donor nuclei creates stronger confinement potentials and enhanced hyperfine couplings. We show theoretically that with atomic precision engineering of the locations of the donor nuclei in these multidonor quantum dot qubits, and/or nuclear spin control, we can minimize the hyperfine mediated relaxation allowing T_1 to extend to ~200 seconds ($B = 1.5$ T).

DOI: 10.1103/PhysRevResearch.5.023043

I. INTRODUCTION

Quantum bits (or qubits) with long-lived quantum states are important for minimizing errors during operations. Electrons bound to phosphorus (P) donors in silicon (Si) have shown exceptionally long spin relaxation times with high fidelity single and two qubit gates [1] due to the strong confinement from the donor potential and weak spin-orbit interaction [2–6]. In the case of a single P donor, spin relaxation measurements have shown $T_1 = 8$ s at $B = 1.25$ T [4,5] [see Fig. 1(a)]. In contrast, multidonor quantum dots with up to three P donors closely packed within the dot have achieved much longer T_1 times of 30 seconds at $B = 1.5$ T [6] [see Fig. 1(b)]. In all these devices the phonon relaxation rate was dominated by a spin-orbit mediated process and observed to follow a B^5 dependency at magnetic fields above ~3 T [7,8], see Figs. 1(a) and 1(b). Interestingly at low magnetic fields, around $B = 1 - 2$ T, a deviation of the relaxation rate from the B^5 behavior has now been observed in multiple devices [3,6,9]. In the case of a single P donor in a metal oxide semiconductor (MOS) architecture this deviated has been observed most markedly in devices where the donor is located close to, and directly beneath, the metal gate that sits above the oxide. Here the presence of evanescent wave Johnson noise (EWJN) from the gate causes spin relaxation since the metal gate constitutes an electromagnetic reservoir that can absorb energy [9]. In contrast, precision placed donor devices using scanning tunneling microscope (STM) lithography are fabricated in a purely crystalline environment in which the charge noise has been found to be very low as there is no metal gate above a dielectric nearby [10,11]. For precision single donor devices the relaxation rate therefore maintained a B^5 dependency down to much lower magnetic fields ($B \sim 1.8$ T), see the black squares in Fig. 1(a). For $B < 1.8$ T, the relaxation rate of a precision single donor device also starts to deviate from the B^5 line. This is most likely due to the remaining charge noise in the system [5,11]. For multidonor quantum dot qubits the low field behavior, however, has been observed to have a B^3 [see Fig. 1(b)] rather than the linear B dependency observed in MOS devices at low magnetic field and the deviation from B^5 behavior starts to occur at $B \sim 2.5 - 3.0$ T [6]. In this paper we investigate what gives rise to the deviation at $B < 3$ T in these multidonor systems and show how we can use this understanding to increase the values of T_1 further in donor based qubits. These results are important since magnetic control of both single and multidonor quantum dot qubits typically occurs at magnetic fields ~1.5 T [12–14].

Since phonons do not carry any spin angular momentum, they alone cannot flip the electron spin to form a spin relaxation channel. To achieve this, we require a coupling mechanism such as the spin-orbit interaction, which mixes the spin and orbital degrees of freedom and produces the coupling between spin and phonons. With donor qubits the hyperfine

*Corresponding author: michelle.simmons@unsw.edu.au

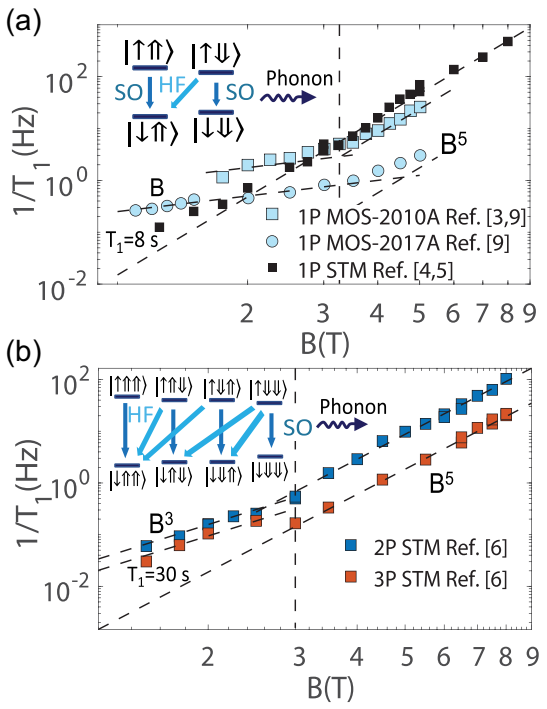

FIG. 1. Spin relaxation rates in single and multidonor quantum dots as a function of external magnetic field, $\boldsymbol{B}$. (a) The relaxation rate of a single donor follows a B^5 dependency in magnetic field and is explained by a spin-orbit (SO) mediated phonon relaxation process represented by the dark blue straight arrows in the inset schematic. The hyperfine mediated phonon relaxation process, shown as HF, is too small to be observed in the measured single donor relaxation rate. B is ‖[110] crystal direction in all three cases. (b) In contrast, in a 2P and 3P multidonor quantum dot we observe a transition from a B^5 dependency at high magnetic field ($B > 3$ T) arising from spin-orbit relaxation, to a B^3 dependency at low magnetic fields due to hyperfine mediated phonon relaxation. The data has been measured with B orientated at 68° with respect to the [100] crystal axis.

interaction between the electron and ^{31}P nuclear spins ($I = 1/2$) can also mix the spin and orbital degrees of freedom as the hyperfine interaction depends on the electron orbital wave function at the donor site. Together with the presence of phonons in the lattice these can form alternate spin relaxation channels.

Similar hyperfine mediated relaxation mechanisms have been investigated in III–V semiconductors such as GaAs quantum dot systems [15–17], II–VI semiconductors such as CdTe/ZnTe quantum dot [18], and donor systems in Si with a nearby interface [19]. In Table I we compare the electron spin relaxation mechanisms of multi-P donor quantum dots in Si with GaAs quantum dot systems. In the low field regime ($B < 3$ T) of the P quantum dot in Si system, as we will show in this work, the hyperfine interaction between the electron spin and ^{31}P donor $I = 1/2$ nuclear spin state dominates the spin-phonon relaxation processes. The spin-relaxation rate has a B^3 dependence due to the magnitude of the deformation potential phonon strain. Similarly, in the low field regime ($B < 2$ T) of the GaAs quantum dot systems, the hyperfine interaction between the electron spin and the ^{69}Ga, ^{71}Ga, and ^{75}As $I = 3/2$ nuclear spin isotopes dominate the spin relaxation rates. However, while the deformation potential phonons mix the valley states of electron in P donors in Si, giving rise to a B^3 dependency, in GaAs quantum dot the absence of valleys result in a higher-order effect with orbital state mixing, giving the spin-relaxation rate due to deformation potential phonons a B^5 dependency [17]. Owing to the piezoelectric nature of the GaAs crystal, piezoelectric phonons therefore dominate with a B^3 dependency to the relaxation rate [17].

In both the P donor dot in Si and GaAs quantum dot systems, the hyperfine interaction mostly depends on the electron density at the nuclear spin sites (contact hyperfine) with the same effect on rotating the external magnetic field. When the magnetic field is not large enough to perturb the electron wave function, changing the magnetic field directions does not influence the electron density at the nuclear spin sites. In addition to the contact hyperfine, however, anisotropic hyperfine is also present due to the dipolar interaction of the electron and nuclear spin. This anisotropic hyperfine is however usually three orders of magnitude smaller than the contact hyperfine in the case of P donors in Si [20–22]. We therefore only consider the contact hyperfine in which the hyperfine mediated spin relaxation is isotropic with respect to the crystal axes in both the donor dot in Si and GaAs quantum dot systems.

In the high magnetic field regime in both systems, the spin-orbit interaction gives an additional B^2 dependence, resulting in a total of B^5 dependency of the phonon relaxation rate. For P in Si systems, recent papers have shown the spin-orbit interaction coupling of the external electric fields with magnetic fields [5] is responsible for the additional B^2 dependence. In GaAs quantum dot systems, the Van-Vleck cancellation [17] results in this additional B^2 dependence. The strength and direction of the electron effective spin-orbit field

TABLE I. Comparison of the electron spin relaxation mechanisms of P donor quantum dots (QDs) in Si with GaAs quantum dot systems in both low and high magnetic field regimes.

	Low field regime ($B < 3$T) P in Si QDs	Low field regime ($B < 2$T) GaAs QDs	High field regime ($B > 3$T) P in Si QDs	High field regime ($B > 2$T) GaAs QDs
$1/T_1$ B dependence	B^3	B^3	B^5	B^5
Dominating phonon mechanism	Deformation potential phonons	Piezoelectric phonons	Deformation potential phonons	Piezoelectric phonons
Origin of spin mixing	Hyperfine	Hyperfine	Spin orbit	Spin orbit
Response to different B field orientations	Isotropic	Isotropic	Anisotropic	Anisotropic

in both the P in Si and GaAs quantum dots changes when rotating the external magnetic field with respect to the crystal axes [5,23,24]. This results in an anisotropic $1/T_1$ magnetic field dependence for the spin-orbit mechanisms.

In this work, we investigate the hyperfine mediated relaxation of both single donor and multidonor quantum dot electron spin qubits at low magnetic fields. In single donor qubits we confirm that the nuclear spin is observed to flip from spin down to spin up at a rate dictated by the hypefine mediated transition of the electron spin and nuclear spin flipflop [25]. This flip-flop process therefore causes spin relaxation and a reduction of T_1. This hyperfine relaxation rate is typically too small to cause a significant deviation of $1/T_1$ from the B^5 line in single donors. On the other hand, the occurrence of this flip-flop process in multiple nuclear spin systems is large enough to cause a transition to a B^3 dependence at low magnetic fields [6]. We use an atomistic tight-binding methodology [26] to quantify the modulation of the hyperfine interaction in these multidonor systems in the presence of deformation potential phonons. The phonon strain couples the ground and excited states of the electrons bound to both single donors and multidonor quantum dots. The hyperfine coupling strength of single electron states can be determined from electron wave functions obtained by the 20-band nearest-neighboir tight-binding Hamiltonian. This tight-binding model has been shown to give an accurate description of the wave function near the donor site, where crystal symmetry is important and central cell corrections take place [26,27].

We consider different atomic configurations of donors within multidonor dots to see what effect the spatial locations of the donors has on the spin relaxation rate. We observe that when the donors are separated far apart (>4 nm), the electron wave function spreads out to a larger extent such that the hyperfine coupling is lower, and the deviation in the hyperfine mediated $1/T_1$ from B^5 is smaller. This tells us that by positioning the donor locations with atomic precision [28] we can engineer the hyperfine coupling to minimize this relaxation process. This result is different to the conclusion of Ref. [8], where putting the donors close together was shown to increase the valley-orbit gap resulting in longer T_1 times. Furthermore, we show that if we can control the orientation of the nuclear spins of each donor using nuclear magnetic resonance (NMR) such that each nuclear spin is in the up spin state, then the electron spin qubit cannot flipflop with any of the nuclear spins and hyperfine relaxation can be completely avoided so that the T_1 time can be extended from 30 s to 223 s.

II. MODELING THE HYPERFINE MEDIATED SPIN RELAXATION

In the inset of Fig. 1(a) we show a schematic energy level diagram of the single P donor with $|\Uparrow\rangle$ and $|\Downarrow\rangle$ nuclear spin states giving rise to two electron spin $|\downarrow\rangle$ to $|\uparrow\rangle$ resonance frequencies. The two dark blue straight arrows show the spin-orbit (SO) coupled electron spin relaxation pathways, in which the P nuclear spin remains unmodified. The electron spin can also relax from the state $|\uparrow\Downarrow\rangle$ to state $|\downarrow\Uparrow\rangle$ through hyperfine coupling, as shown as the cross arrow HF resulting in a concomitant nuclear spin flip. In the inset of Fig. 1(b) we consider the multiple relaxation pathways now present for a

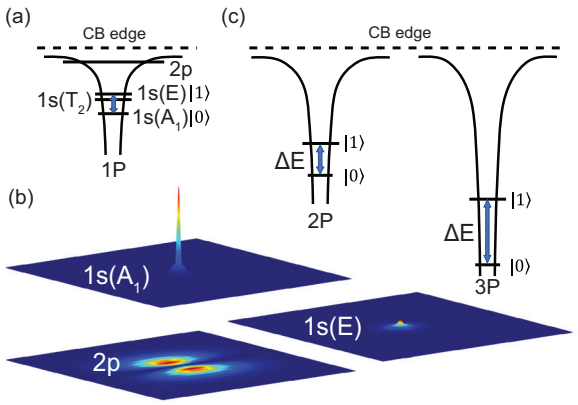

FIG. 2. Comparison between the energy levels and energy splittings of a single (1P), a two (2P), and a three (3P) donor quantum dot qubit. (a) Energy level diagram of a single donor with respect to the Si conduction band (CB) edge. The ground state [$1s(A_1)$]) couples with the excited $1s(E)$ doublet state through both the hyperfine interaction and deformation potential phonons. (b) The calculated electron wave function of the 1P donor, obtained from an atomistic tight-binding method. The electron probability density (represented by the height of each graph) at the center donor site changes drastically as we go from $1s(A_1)$ (maximum height is scaled to be one) to $1s(E)$ [maximum height is 0.086 relative to the $1s(A_1)$ maximum height], then to $2p$ states (almost zero density at the center). (c) The energy levels and splittings between the ground $|0\rangle$ and first excited states $|1\rangle$ of the 2P and 3P systems.

2P donor quantum dot. With two P nuclear spins, there are four possible initial states for electron spin up and four possible final states for electron spin down. We therefore have four SO transitions shown by the dark blue arrows. Each P nuclear spin can also flipflop with the electron spin, with the other nuclear spin pointing either up or down, resulting in a total of four HF transitions shown by the light blue crossarrows.

To calculate the hyperfine mediated spin relaxation rates it is important to determine which orbital states in donor systems contribute, see Fig. 2(a). The ground state of an electron bound to a single donor has a $1s$ envelope function with A_1 valley symmetry, followed by a triplet T_2 and doublet E excited state, each with a $1s$ envelope function [29]. The $1s(T_2)$ triplet state does not contribute to the hyperfine mediated spin relaxation rate [7] since it is composed of $+k_i$ and $-k_i$ valleys ($i = x$, y, or z), whilst the deformation potential operator [8] in H_{ep} acts as a constant on the two $+k_i$ and $-k_i$ valleys, such that $1s(T_2)$ cannot couple with the $1s(A_1)$ state ($\langle 1s(A_1)|H_{ep}|1s(T_2)\rangle \sim \langle 1s(A_1)|1s(T_2)\rangle = 0$). The $2p$ donor states are also much higher up in energy and have very small hyperfine splittings since the $2p$ wave function has a zero density at the center [see Fig. 2(b)]. As a consequence only the two $1s(E)$ states couple to the $1s(A_1)$ states and are included in our calculations.

In the single donor case the $1s(T_2)$ state does not contribute to the relaxation process. In multidonor dots with random separation axis between the donors, the symmetry of the system is lowered by the presence of other donors, with the valley states having a mixture of $\pm k_x$, $\pm k_y$, and $\pm k_z$ valleys, such that in general the deformation potential operator can no longer be treated as a constant. Now the electron-phonon Hamiltonian

can have a nonzero matrix element between the ground and the next higher energy state [see Fig. 2(c)].

After determining the states which contribute to the spin relaxation processes, we now calculate the corresponding hyperfine coupling strengths and resulting relaxation rates. In multidonor systems, each hyperfine transition can be independently treated theoretically in the same way as for the hyperfine transition of a single donor since only one nuclear spin flips each time. For simplicity, we focus on the flipping nuclear spin in the following equations.

The hyperfine mediated electron spin relaxation rate $1/T_1$ of these ground spin states $|0\uparrow\Downarrow'\rangle$ and $|0\downarrow\Uparrow'\rangle$, split by the Zeeman energy E_Z, can be obtained from Fermi's Golden Rule:

$$\frac{1}{T_1} = \frac{2\pi}{\hbar}|\langle 0\downarrow\Uparrow'|H_{ep}|0\uparrow\Downarrow'\rangle|^2\delta(E_Z-\hbar\omega_q), \tag{1}$$

where H_{ep} is the electron-phonon Hamiltonian and ω_q is the angular frequency of the emitted phonon. H_{ep} can couple the same electron/nuclear spin states but in different orbitals, whereas the hyperfine interaction, H_{HF}, couples both different orbitals as well as different electron/nuclear spin states. The perturbed ground state $|0\uparrow\Downarrow'\rangle$ mixed by the hyperfine interaction is given by $|0\uparrow\Downarrow'\rangle \sim |0\uparrow\Downarrow\rangle + \frac{\langle 1\downarrow\Uparrow|H_{HF}|0\uparrow\Downarrow\rangle}{\Delta E}|1\downarrow\Uparrow\rangle$ and

$$\langle 0\downarrow\Uparrow'|H_{ep}|0\uparrow\Downarrow'\rangle \sim \frac{1}{\Delta E}\langle 0\downarrow\Uparrow|H_{ep}|1\downarrow\Uparrow\rangle\langle 1\downarrow\Uparrow|H_{HF}|0\uparrow\Downarrow\rangle, \tag{2}$$

where ΔE is the energy splitting between the ground state $|0\rangle$ and the higher orbital state $|1\rangle$.

The hyperfine Hamiltonian H_{HF} is given by [22,30]

$$H_{HF} = \frac{\mu_0}{4\pi}g_e\mu_B g_n\mu_n\frac{8\pi}{3}I\,S\delta^3(r) + \frac{\mu_0}{4\pi}g_e\mu_B g_n\mu_n\frac{3(I\ \hat{r})(S\,\hat{r})-I\ S}{r^3}, \tag{3}$$

where g_e and g_n are the electron and nuclear g factors, respectively,;μ_B and μ_n are the Bohr magneton and nuclear magneton, respectively; μ_0 is the vacuum permeability; I is the nuclear spin operator and S is the electron spin operator; and $\vec{r} = r\hat{r}$ is the vector joining the electron and nuclear spin. The first term is the Fermi-contact hyperfine, resulting from the magnetic interaction between the electron spin and the P nuclei. This becomes significant when there is an unpaired electron spin at the nucleus. The second term is the anisotropic hyperfine which results from the dipolar interaction between the electron spin and the nuclear spin. Since the resulting energy splitting of the anisotropic hyperfine is threeorders of magnitude smaller than the Fermi-contact hyperfine in single donors [20,21], we only need to consider the contact hyperfine in our calculations. Substituting the corresponding H_{HF} in Eq. (2), gives the matrix element

$$\langle 1\downarrow\Uparrow|H_{HF}|0\uparrow\Downarrow\rangle = C\psi_0^*(r_0)\psi_1(r_0), \tag{4}$$

$C = 2\frac{\mu_0}{4\pi}g_e\mu_B g_n\mu_n\frac{8\pi}{3}$. Here r_0 is the donor location. The relaxation rate, $1/T_1$, is proportional to the product of the ground and higher orbital states hyperfine splittings A_0 and A_1 :

$$\frac{1}{T_1} \sim |\langle 1\downarrow\Uparrow|H_{HF}|0\uparrow\Downarrow\rangle|^2 = C^2|\psi_0(r_0)|^2|\psi_1(r_0)|^2 = \frac{1}{4}A_0A_1. \tag{5}$$

The electron wave functions of the P donors in crystalline Si are obtained by constructing the nearest neighbor tight-binding Hamiltonian within a 20-band $sp^3d^5s^*$ basis. Including all $sp^3d^5s^*$ atomic orbitals is necessary to reproduce the band structure through the Brillouin zone capturing the bandgap and the X-valley transverse mass of bulk Si crystal [31–33]. The spin-orbit interaction in Si is included by considering the atomic spin-orbit coupling between the p-atomic orbitals, following the method from Ref. [34]. Coulomb potentials with a cutoff value U_0 at the center, representing the central-cell correction, are added to the Hamiltonian. We note the onsite tight-binding parameters of the P atom have been fine tuned to capture the measured binding energies of the six $1s$ valley states [35,36]. The resulting degeneracy and valley weights of the six $1s$ states also agree with existing literature [29,37]. This model has successfully captured the quadratic Stark tuning of donor hyperfine coupling [26,38] and explained the hyperfine values in a two-donor quantum dot [39]. The bulk donor hyperfine value of the $1s(A_1)$ state is $A_0 = 117.53$ MHz [40]. The hyperfine values of higher orbital states are given by $A_1 = A_0\frac{|\psi_1(r_0)|^2}{|\psi_0(r_0)|^2}$ and the hyperfine values of multidonor quantum dots are obtained in the same way. The resulting hyperfine value of the doublet $1s(E)$ state, $A_1 = 10.10$ MHz, is much smaller than the ground $1s(A_1)$ state ($A_0 = 117.53$ MHz) since the electron density at the donor site is lower, with the highest density being in the $1s(A_1)$ state [see Fig. 2(b)].

To determine the total hyperfine mediated phonon relaxation rate $(1/T_1)_{HF}$, we know $(1/T_1)_{HF} = KB^3|H_{HF}|^2$, where KB^3 contains the energy gap ΔE between the coupling states and the electron-phonon coupling, and H_{HF} is the hyperfine coupling strength [see Eq. (2)]. This gives $(1/T_1)_{HF}$ a B^3 dependency since H_{HF} is independent of B. We determine the KB^3 term from existing spin-orbit $1/T_1$ measurements [3–6] and the corresponding spin-orbit strength [5]. This is because the spin-orbit mediated phonon relaxation rate $(1/T_1)_{SO} = KB^3|H_{SO}|^2$ shares the same KB^3 with the hyperfine mediated phonon relaxation rate. We therefore obtain KB^3 by dividing $(1/T_1)_{SO}$ by $|H_{SO}|^2$. In Ref. [5], we show that while the KB^3 term is isotropic to external magnetic field orientations, H_{SO} changes its magnitude with different magnetic field orientations, causing the single donor $(1/T_1)_{SO}$ to be anisotropic. In Fig. 1(a), the $(1/T_1)_{SO}$ data from Ref. [4,5] has been measured with the magnetic field along the [110] crystal direction, so we can extract the strength of H_{SO} to obtain the single donor KB^3. The KB^3 term of a 2P and 3P multi-donor quantum dot can be extracted from $(1/T_1)_{SO}$ in Fig. 1(b) which has a magnetic field oriented at 68° with respect to the [100] crystal direction as in the experiment [6].

III. COMPARISON TO EXPERIMENTAL RESULTS AND MINIMIZING THE HYPERFINE MEDIATED SPIN RELAXATION

A. Single donors

In Table II, we compare the hyperfine mediated spin relaxation rate $(1/T_1)_{HF}$ of the electron spin obtained from our model with recent measurements of the nuclear spin flip relaxation rate in a single donor MOS device [25]. This allows us to determine if the electron spin does indeed flip-flop

TABLE II. Comparison of the hyperfine mediated spin relaxation rate from our model with the measured nuclear spin down-to-up flip rate in a single donor MOS device at $B = 1.77$ T and $T < 1$ K.

Hyperfine mediated $1/T_1$ (our model)	0.0087 ± 0.0003 Hz
Measured nuclear spin down-to-up flip rate [25]	0.0154 ± 0.01 Hz

with the nuclear spin at the same rate. Here we see that at $B = 1.77$ T the hyperfine mediated rate obtained from our model is less than a factor of two different from the measured nuclear flip rate, within the error bars of the measurements [25]. Significantly, the hyperfine mediated electron relaxation rate, $(1/T_1)_{HF} = 0.0087$ Hz is much smaller than the EWJN induced electron relaxation rates observed in MOS devices, which range from 0.15 to 2 Hz at $B = 1.77$ T [9]. The hyperfine mediated electron relaxation rate, $(1/T_1)_{HF} = 0.0087$ Hz, is also more than one order of magnitude smaller than the spin-orbit mediated relaxation rate, $(1/T_1)_{SO} = 0.2606$ Hz [3–5] at $B = 1.77$ T. We can therefore conclude that in a single donor device it will not be possible to directly observe the hyperfine relaxation rate from electron T_1 measurements when $B > 1$ T [3–5,9].

B. Multidonor dots

The spin relaxation in multidonor dots such as 2P $(1/T_1)_{SO}$ is an order of magnitude smaller than the single donor 1P $(1/T_1)_{SO}$ (see Fig. 1). This result is a consequence of the larger energy splitting between the coupling states in the 2P dot due to the stronger confinement potential which yields a smaller $(1/T_1)_{SO}$ [8]. In contrast the 2P $(1/T_1)_{HF}$ can be an order of magnitude larger than 1P $(1/T_1)_{HF}$ since the electron wave function is now more localized in a multidonor quantum dot due to the deeper Coulomb potential pulling the electron wavefunction into the core [8,22]. As a consequence the ground state hyperfine constant for a two-donor quantum dot (depending on the exact locations of the donors within the dot) can reach a much larger hyperfine value $A = 366$ MHz, compared to the bulk single donor value, $A = 117.53$ MHz [22]. With more donors there are also more nuclear spins for the electron spin to flipflop with, leading to a further increase in the total spin relaxation rate. Charge noise in precision donor devices in crystalline silicon is very low [10,11] in contrast to MOS devices where EWJN dominates with a linear B dependency at low magnetic fields [9]. As a consequence in multidonor quantum dots the hyperfine mediated relaxation mechanism thus becomes the dominant relaxation mechanism at low magnetic fields where the spin qubit operates.

Figure 3 shows a comparison of the calculated and measured electron spin relaxation rate for multidonor quantum dots that contain two (2P) and three (3P) donor atoms as a function of magnetic field B. The red lines in Figs. 3(a) and 3(b) represent the B^5 $(1/T_1)_{SO}$ spin relaxation process. We calculate the relaxation rate $SO + HF$ by considering all possible relaxation pathways [there are a total of eight pathways for a 2P dot, see inset of Fig. 1(b), and 20 pathways for a 3P dot], from all possible initial spin configurations (equally weighted). We assume all initial nuclear spin orientations within the 2P and 3P dots are equally populated as they follow the Boltzmann distribution at $T = 100$ mK [6] ($K_BT = 8.6$ μeV), with a nuclear Zeeman (~0.1 μeV at $B = 2$ T) and hyperfine difference between different nuclear spin configurations $(A_0/2)$ ~0.7 μeV.

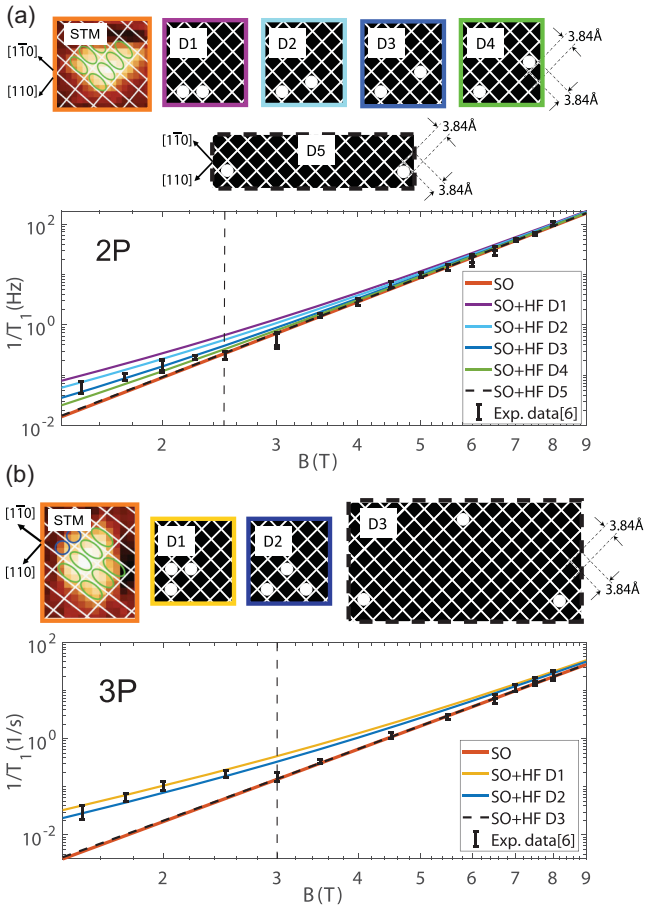

FIG. 3. Importance of hyperfine mediated phonon relaxation in multidonor quantum dots. The observed deviation of the spin relaxation rate to a B^5 dependence with magnetic field [6] can be explained by considering the hyperfine mediated relaxation rates and adding them to the spin-orbit mediated relaxation rates. (a) Electron bound to a 2P donor quantum dot with five different configurations from D1 to D5. (b) Electron bound to a 3P donor quantum dot with three different configurations D1, D2, and D3. The experimental data has been measured with B oriented at 68° with respect to the [100] crystal axis.

We consider multiple different configurations of the donor atoms within the lithographic patch of the quantum dot patterned by STM [6], D1–D4 [see Fig. 3(a)]. From this we can see that for the 2P case, the D3 configuration (dark blue line) where the donors are 1.21 nm apart is consistent with the relaxation rate deviation observed, experimentally represented by the vertical error bars. The closest interdonor configuration (D1 purple line) with the donors 0.54 nm apart has the strongest hyperfine coupling as the electron wave function is strongly confined and results in the largest deviation from the spin-orbit relaxation (red line). In contrast, the D4 farthest

interdonor configuration (green line) with the donors 1.58 nm apart has the least deviation from the red line.

To see if we can minimize the hyperfine relaxation further, we separated the two donors along [100] by 4.89 nm {[D5 in Fig. 3(a)]. Here the hyperfine value of each donor reaches a minimum $A_0 = 52.94$ MHz, as shown in Ref. [22]. The corresponding 2P $(1/T_1)_{HF} = 0.0018$ Hz at $B = 1.5$ T, is now much smaller than $(1/T_1)_{SO} = 0.0213$ Hz at $B = 1.5$ T [extracted from the red line in Fig. 3(a), assuming D5 $(1/T_1)_{SO}$ is similar to the red line]. The total relaxation rate, as shown in the black dashed line in Fig. 3(a), now shows almost no deviation from the B^5 behavior indicating that we can minimize the hyperfine mediated spin relaxation process. Furthermore, the 2P (D5) hyperfine relaxation rate, $(1/T_1)_{HF} = 0.0029$ Hz at $B = 1.77$ T, is smaller than the 1P hyperfine relaxation rate $(1/T_1)_{HF} = 0.0087$ Hz at $B = 1.77$ T, as shown in Table I, in contrast to a closely spaced 2P where $(1/T_1)_{HF}$ is much larger. With current STM patterning technology [28], it should be possible to engineer donor locations to achieve $T_1 = 45$ s (extracted from the black dashed line), compared to the currently measured values of $T_1 = 15$ s at $B = 1.5$ T [6].

For the 3P case, both D1 (yellow line) and D2 (dark blue line) represent configurations, in which the donors are placed within the lithography patch [see Fig. 3(b)] with separations between the three donors of 0.77 and 1.09 nm. They both provide a consistent fit with the measured $1/T_1$ deviation. As with the 2P case, we can increase the separation between the three donors to $\sim 4-5$ nm, as shown in D3 in Fig. 3(b), where now the hyperfine relaxation rate $(1/T_1)_{HF} = 0.0007$ Hz at $B = 1.5$ T becomes very small. Here we have minimized the hyperfine mediated relaxation process and the total relaxation rate (black dashed line) follows the red line in Fig. 3(b), giving T_1 times $\sim$207 s, much longer than the currently measured values of 30 s at $B = 1.5$ T [6].

Importantly, we find that we can also completely switch off the hyperfine mediated spin relaxation by fixing the nuclear spins into well known states making the hyperfine transition forbidden. If the nuclear spins are controlled and fixed at the $|\uparrow\Uparrow\Uparrow\rangle$ state for the 2P and $|\uparrow\Uparrow\Uparrow\Uparrow\rangle$ state for the 3P donor quantum dot, the hyperfine transitions HF are no longer allowed since there are no down nuclear spins to flipflop with the up electron spin [see inset of Fig. 1(b)]. In this case at low magnetic fields the relaxation rate will directly follow the red lines in Fig. 3, giving T_1 times up to 223 s at $B = 1.5$ T. Initializing the nuclear spin states to set configurations should be possible using nuclear spin control methods such as NMR [25] and dynamic nuclear polarization (DNP) [41–43].

IV. CONCLUSION

To conclude, we use a 20 band $sp^3d^5s^*$ atomistic tight-binding Hamiltonian model to calculate hyperfine mediated relaxation of the electron spin in multidonor qubits. We show that the deviation of the $1/T_1$ relaxation rate from B^5 to B^3 at low magnetic fields for both a 2P and 3P multidonor quantum dot qubit arise due to the hyperfine mediated phonon relaxation. We show that by positioning the donors $4-5$ nm apart we can minimize the hyperfine relaxation rate to achieve T_1 times of 45 s for 2P and 207 s for 3P, at $B = 1.5$ T. Additionally, by initializing the nuclear spin to well known configurations $|\uparrow\Uparrow\Uparrow\rangle$ and $|\uparrow\Uparrow\Uparrow\Uparrow\rangle$, the electron cannot flipflop with any of the nuclear spins in these dots, thereby further suppressing this hyperfine coupling and leading to T_1 values of 223 s in a 3P donor quantum dot at magnetic fields $B = 1.5$ T where donor qubits are operated.

ACKNOWLEDGMENTS

This research was conducted by the Australian Research Council Centre of Excellence for Quantum Computation and Communication Technology (CE170100012), the US Army Research Office under Contract No. W911NF-17-1-0202, and Silicon Quantum Computing Pty Ltd. M.Y.S. acknowledges an Australian Research Council Laureate Fellowship.

The research was undertaken with the assistance of resources and services from the National Computational Infrastructure (NCI) under NCMAS 2020 and 2021 allocation, supported by the Australian Government, and of the computational cluster Katana supported by Research Technology Services at UNSW Sydney.

[1] M. T. Mądzik, S. Asaad, A. Youssry, B. Joecker, K. M. Rudinger, E. Nielsen, K. C. Young, T. J. Proctor, A. D. Baczewski, A. Laucht *et al.*, Precision tomography of a three-qubit donor quantum processor in silicon, Nature (London) **601**, 348 (2022).

[2] D. K. Wilson and G. Feher, Electron spin resonance experiments on donors in silicon. III. investigation of excited states by the application of uniaxial stress and their importance in relaxation processes, Phys. Rev. **124**, 1068 (1961).

[3] A. Morello, J. J. Pla, F. A. Zwanenburg, K. W. Chan, K. Y. Tan, H. Huebl, M. Möttönen, C. D. Nugroho, C. Yang, J. A. van Donkelaar *et al.*, Single-shot readout of an electron spin in silicon, Nature (London) **467**, 687 (2010).

[4] T. F. Watson, B. Weber, M. G. House, H. Büch, and M. Y. Simmons, High-Fidelity Rapid Initialization and Read-Out of an Electron Spin Via the Single Donor D- Charge State, Phys. Rev. Lett. **115**, 166806 (2015).

[5] B. Weber, Y.-L. Hsueh, T. F. Watson, R. Li, A. R. Hamilton, L. C. L. Hollenberg, R. Rahman, and M. Y. Simmons, Spin–orbit coupling in silicon for electrons bound to donors, npj Quantum Inf. **4**, 61 (2018).

[6] T. F. Watson, B. Weber, Y.-L. Hsueh, L. C. L. Hollenberg, R. Rahman, and M. Y. Simmons, Atomically engineered electron spin lifetimes of 30 s in silicon, Sci. Adv. **3**, e1602811 (2017).

[7] H. Hasegawa, Spin-lattice relaxation of shallow donor states in Ge and Si through a direct phonon process, Phys. Rev. **118**, 1523 (1960).

[8] Y.-L. Hsueh, H. Büch, Y. Tan, Y. Wang, L. C. L. Hollenberg, G. Klimeck, M. Y. Simmons, and R. Rahman, Spin-Lattice Relaxation Times of Single Donors and Donor Clusters in Silicon, Phys. Rev. Lett. **113**, 246406 (2014).

[9] S. B. Tenberg, S. Asaad, M. T. Mądzik, M. A. I. Johnson, B. Joecker, A. Laucht, F. E. Hudson, K. M. Itoh, A. M. Jakob, B. C. Johnson, D. N. Jamieson, J. C. McCallum, A. S.

Dzurak, R. Joynt, and A. Morello, Electron spin relaxation of single phosphorus donors in metal-oxide-semiconductor nanoscale devices, Phys. Rev. B **99**, 205306 (2019).

[10] S. Shamim, B. Weber, D. W. Thompson, M. Y. Simmons, and A. Ghosh, Ultralow-noise atomic-scale structures for quantum circuitry in silicon, Nano Lett. **16**, 5779 (2016).

[11] L. Kranz, S. K. Gorman, B. Thorgrimsson, Y. He, D. Keith, J. G. Keizer, and M. Y. Simmons, Exploiting a single-crystal environment to minimize the charge noise on qubits in silicon, Adv. Mater. **32**, 2003361 (2020).

[12] J. J. Pla, K. Y. Tan, J. P. Dehollain, W. H. Lim, J. J. Morton, D. N. Jamieson, A. S. Dzurak, and A. Morello, A single-atom electron spin qubit in silicon, Nature (London) **489**, 541 (2012).

[13] J. T. Muhonen, J. P. Dehollain, A. Laucht, F. E. Hudson, R. Kalra, T. Sekiguchi, K. M. Itoh, D. N. Jamieson, J. C. McCallum, A. S. Dzurak *et al.*, Storing quantum information for 30 seconds in a nanoelectronic device, Nat. Nanotechnol. **9**, 986 (2014).

[14] L. Fricke, S. J. Hile, L. Kranz, Y. Chung, Y. He, P. Pakkiam, M. G. House, J. G. Keizer, and M. Y. Simmons, Coherent control of a donor-molecule electron spin qubit in silicon, Nat. Commun. **12**, 3323 (2021).

[15] A. Khaetskii, D. Loss, and L. Glazman, Electron spin evolution induced by interaction with nuclei in a quantum dot, Phys. Rev. B **67**, 195329 (2003).

[16] S. I. Erlingsson and Y. V. Nazarov, Hyperfine-mediated transitions between a Zeeman split doublet in GaAs quantum dots: The role of the internal field, Phys. Rev. B **66**, 155327 (2002).

[17] L. C. Camenzind, L. Yu, P. Stano, J. D. Zimmerman, A. C. Gossard, D. Loss, and D. M. Zumbühl, Hyperfine-phonon spin relaxation in a single-electron GaAs quantum dot, Nat. Commun. **9**, 3454 (2018).

[18] C. Le Gall, A. Brunetti, H. Boukari, and L. Besombes, Electron-nuclei spin dynamics in II–VI semiconductor quantum dots, Phys. Rev. B **85**, 195312 (2012).

[19] P. Boross, G. Széchenyi, and A. Pályi, Valley-enhanced fast relaxation of gate-controlled donor qubits in silicon, Nanotechnology **27**, 314002 (2016).

[20] E. B. Hale and R. L. Mieher, Shallow donor electrons in silicon. I. hyperfine interactions from endor measurements, Phys. Rev. **184**, 739 (1969).

[21] S. H. Park, R. Rahman, G. Klimeck, and L. C. L. Hollenberg, Mapping Donor Electron Wave Function Deformations at a Sub-Bohr Orbit Resolution, Phys. Rev. Lett. **103**, 106802 (2009).

[22] Y. Wang, C.-Y. Chen, G. Klimeck, M. Y. Simmons, and R. Rahman, Characterizing Si:P quantum dot qubits with spin resonance techniques, Sci. Rep. **6**, 31830 (2016).

[23] S. D. Ganichev and L. E. Golub, Interplay of rashba/dresselhaus spin splittings probed by photogalvanic spectroscopy–a review, Phys. Status Solidi B **251**, 1801 (2014).

[24] P. Scarlino, E. Kawakami, P. Stano, M. Shafiei, C. Reichl, W. Wegscheider, and L. M. K. Vandersypen, Spin-Relaxation Anisotropy in a GaAs Quantum Dot, Phys. Rev. Lett. **113**, 256802 (2014).

[25] J. J. Pla, K. Y. Tan, J. P. Dehollain, W. H. Lim, J. J. Morton, F. A. Zwanenburg, D. N. Jamieson, A. S. Dzurak, and A. Morello, High-fidelity readout and control of a nuclear spin qubit in silicon, Nature (London) **496**, 334 (2013).

[26] R. Rahman, C. J. Wellard, F. R. Bradbury, M. Prada, J. H. Cole, G. Klimeck, and L. C. L. Hollenberg, High Precision Quantum Control of Single Donor Spins in Silicon, Phys. Rev. Lett. **99**, 036403 (2007).

[27] M. Friesen, Theory of the Stark Effect for P Donors in Si, Phys. Rev. Lett. **94**, 186403 (2005).

[28] M. Fuechsle, J. A. Miwa, S. Mahapatra, H. Ryu, S. Lee, O. Warschkow, L. C. L. Hollenberg, G. Klimeck, and M. Y. Simmons, A single-atom transistor, Nat. Nanotechnol. **7**, 242 (2012).

[29] W. Kohn and J. Luttinger, Theory of donor states in silicon, Phys. Rev. **98**, 915 (1955).

[30] D. J. Griffiths and D. F. Schroeter, *Introduction to Quantum Mechanics* (Cambridge University Press, 2018)

[31] P. Vogl, H. P. Hjalmarson, and J. D. Dow, A semi-empirical tight-binding theory of the electronic structure of semiconductors, J. Phys. Chem. Solids **44**, 365 (1983).

[32] J.-M. Jancu, R. Scholz, F. Beltram, and F. Bassani, Empirical spds* tight-binding calculation for cubic semiconductors: General method and material parameters, Phys. Rev. B **57**, 6493 (1998).

[33] T. B. Boykin, G. Klimeck, and F. Oyafuso, Valence band effective-mass expressions in the sp3d5s* empirical tight-binding model applied to a Si and Ge parametrization, Phys. Rev. B **69**, 115201 (2004).

[34] D. Chadi, Spin-orbit splitting in crystalline and compositionally disordered semiconductors, Phys. Rev. B **16**, 790 (1977).

[35] S. Ahmed, N. Kharche, R. Rahman, M. Usman, S. Lee, H. Ryu, H. Bae, S. Clark, B. Haley, M. Naumov *et al.*, Multimillion atom simulations with NEMO3D, in *Encyclopedia of Complexity and Systems Science* (Springer, 2009), pp. 5745–5783.

[36] A. Ramdas and S. Rodriguez, Spectroscopy of the solid-state analogues of the hydrogen atom: donors and acceptors in semiconductors, Rep. Prog. Phys. **44**, 1297 (1981).

[37] A. J. Mayur, M. D. Sciacca, A. K. Ramdas, and S. Rodriguez, Redetermination of the valley-orbit (chemical) splitting of the 1s ground state of group-V donors in silicon, Phys. Rev. B **48**, 10893 (1993).

[38] A. J. Sigillito, A. M. Tyryshkin, J. W. Beeman, E. E. Haller, K. M. Itoh, and S. A. Lyon, Large stark tuning of donor electron spin qubits in germanium, Phys. Rev. B **94**, 125204 (2016).

[39] S. J. Hile, L. Fricke, M. G. House, E. Peretz, C. Y. Chen, Y. Wang, M. Broome, S. K. Gorman, J. G. Keizer, R. Rahman, and M. Y. Simmons, Addressable electron spin resonance using donors and donor molecules in silicon, Sci. Adv. **4**, eaaq1459 (2018).

[40] G. Feher, Electron spin resonance experiments on donors in silicon. I. electronic structure of donors by the electron nuclear double resonance technique, Phys. Rev. **114**, 1219 (1959).

[41] A. Abragam and M. Goldman, Principles of dynamic nuclear polarisation, Rep. Prog. Phys. **41**, 395 (1978).

[42] M. Gullans, J. J. Krich, J. M. Taylor, H. Bluhm, B. I. Halperin, C. M. Marcus, M. Stopa, A. Yacoby, and M. D. Lukin, Dynamic Nuclear Polarization in Double Quantum Dots, Phys. Rev. Lett. **104**, 226807 (2010).

[43] S. Simmons, R. M. Brown, H. Riemann, N. V. Abrosimov, P. Becker, H.-J. Pohl, M. L. Thewalt, K. M. Itoh, and J. J. Morton, Entanglement in a solid-state spin ensemble, Nature (London) **470**, 69 (2011).